Three Residues Predicted by Molecular Modeling To Interact with the Purine Moiety Alter Ligand Binding and Channel Gating in Cyclic Nucleotide-Gated Channels†

Sean-Patrick Scott and Jacqueline C. Tanaka*

Department of Pathology, School of Dental Medicine, University of Pennsylvania, Philadelphia, Pennsylvania 19104

Received May 20, 1998; Revised Manuscript Received October 5, 1998

ABSTRACT: Cytoplasmic cAMP and cGMP are soluble cellular messengers that directly activate cyclic nucleotide-gated (CNG) channels. These channels mediate sensory transduction in photoreceptors and olfactory neurons. The closely related CNG channels in these cell types have different nucleotide activation profiles, and we have investigated the molecular basis of their nucleotide selectivity properties. Previously, we predicted that the purine moiety of the nucleotide interacts with residues F533, K596, and D604 (bovine rod α CNG channel subunit sequences) of the nucleotide binding domain. In this study, we replaced these three residues with the corresponding residues of the bovine olfactory CNG channel. Mutations at each position altered the nucleotide activation of the rod CNG channels. In a mutant where K596 was replaced with arginine, cAMP-activated currents were enhanced 8−12-fold, suggesting that residue 596 influences channel gating. Thermodynamic cycle analysis of the data showed that (1) the residues are energetically coupled and (2) energetic coupling exists between the potentiating effects of Ni^{2+} and the replacement of F533 with tyrosine. These data suggest that changes in one of the residues alter the purine contacts with the other residues and that F533 communicates with the C-linker region of the channel involved in Ni^{2+} potentiation.

Cyclic nucleotide-gated (CNG)[1] ion channels were first identified in retinal rods where they transduce light-activated changes in cytoplasmic cGMP levels into voltage changes across the outer segment membrane (*1*). Each subunit in the tetrameric channel has a cGMP binding site at the cytoplasmic surface of the channel, and the cooperative binding of multiple cGMP molecules promotes channel opening (see refs *2* and *3* for reviews). Olfactory neurons have a similar CNG channel which enables cAMP to transduce olfactory stimuli into voltage signals (*4*, *5*). Photoreceptor CNG channels discriminate between cGMP and cAMP with $K_{0.5}$ values for current activation in excised patches that are ∼60-fold lower for cGMP than for cAMP. In addition to the relatively low affinity, cAMP is a partial agonist in photoreceptor channels, activating a small fraction of the total cGMP-activated current at saturating concentrations (*6*). Olfactory channels are fully activated by both cGMP and cAMP at concentrations that are lower than needed to activate photoreceptor channels. The olfactory channels in some species are activated by cGMP and cAMP at similar concentrations (*7*), while in other species, cGMP activates at lower concentrations than cAMP (*8*−*10*). CNG channels are also found in many nonsensory cells, including retinal bipolar (*11*) and ganglion neurons (*12*), heart (*13*), and sperm (*14*), as well as hippocampal (*15*) and pineal neurons (*16*; see ref *3* for review). CNG channels conduct both Na^+ and Ca^{2+}, and although their functional roles are not yet understood in nonsensory cells, these channels might provide an important voltage-independent Ca^{2+} channel for Ca^{2+}-activated cell signaling (*17*).

The topology of CNG channel subunits and the tetrameric organization of CNG channels is similar to that of the large voltage-activated Shaker K channel family (*18*). The general subunit architecture of this family has six transmembrane-spanning domains, S1−S6, a pore region located between S5 and S6, and cytoplasmic N-terminal and C-terminal domains (see refs *2* and *3* for reviews). In CNG channels, the N-terminal region is highly variable between family members and between the two subunit types, denoted α and β or 1 and 2. This region plays a major role in channel gating and accounts for many of the differences in the channel open probabilities between the olfactory and rod channels (*19*, *20*). The C-linker region of the channel which links the final S6 transmembrane region to the cyclic nucleotide binding domain is also a major determinant of channel gating (*8*).

† This work was supported by NIH Grants EY-06640 (J.C.T.) and EY-07035 (training grant for S.-P.S.).

* To whom correspondence should be addressed: Department of Pathology, School of Dental Medicine, 326 Levy Building, 4010 Locust St., University of Pennsylvania, Philadelphia, PA 19104-6002. Phone: (215) 898-4769. Fax: (215) 573-2050. E-mail: tanaka@athens.dental.upenn.edu.

[1] Abbreviations: CNG, cyclic nucleotide-gated; cGMP, cyclic guanosine 3′−5′-monophosphate; cAMP, cyclic adenosine 3′−5′-monophosphate; F533Y, mutant of bovine rod CNGC whereY corresponds to the single-letter abbreviation for the substituted residue and F is the single-letter abbreviation for the wild-type residue; K596R, mutant where Arg is substituted for the wild-type Lys residue; D604E, mutant where Glu is substituted for Asp in position 604. The double mutations include F533Y/K596R, F533Y/D604E, and K596R/D604E. The triple mutation is F533Y/K596R/D604E. Bovine olfactory residues Y510, T537, R573, and E581 correspond to bovine rod residues 533, 560, 596, and 604, respectively.

10.1021/bi981185d CCC: $15.00
Published on Web 11/12/1998

The C-terminal region of the CNG channel has a highly conserved ~120-amino acid cyclic nucleotide binding domain (*21*). This binding domain belongs to the family of structurally similar cyclic nucleotide binding domains that include the bacterial transcription factor cAMP regulatory protein, CRP, and the cGMP-activated (PKG) and cAMP-activated (PKA) protein kinases (*22*, *23*). The coordinates of the co-crystallized structure of cAMP bound to CRP (*24*, *25*) were used previously to construct molecular models of the nucleotide binding domains of both rod and olfactory CNG channels (*26*−*28*). Since cGMP and cAMP differ only at the C2 and C6 positions of the purine, contacts between the C2 and C6 substituents and the binding domain must enable the channels to distinguish between these nucleotides. Our models predicted four residues that could interact with the purine and dictate its conformation, including residues at positions 533, 560, 596, and 604 (bovine rod α subunit numbering). In the model, F533 on the β5 strand of the eight-stranded β roll of the binding domain interacts with the purine through a polar-ring interaction (*26*). In the bovine olfactory α subunit model, the equivalent residue is Y510 which was predicted to interact more strongly with the purine than F533 because of additional contacts mediated by the hydroxyl group (*27*). T560, located on the β7 strand and conserved in all members of the channel family, was predicted to interact with the ribofuranose of both cAMP and cGMP and the guanine, but not adenine, through a hydrogen bond between the C2 amino group on the guanine and the hydroxyl side chain of the amino acid. This prediction was supported experimentally by substituting either serine, which reduced the $K_{0.5}$ for cGMP, or alanine, which greatly increased the $K_{0.5}$ for cGMP (*9*). Our modeling showed that R573 on the C α helix of the bovine olfactory channel interacted with both cGMP and cAMP while K596 of the bovine rod channel was too short to interact with either purine. The charged carboxyl groups of D604 in the bovine rod channel and E581 in the bovine olfactory channel, located at the termination of the C α helix, were predicted to interact with N1 of cGMP through a strong electrostatic interaction.

The purpose of this study was to test the role of bovine rod residues 533, 596, and 604 in determining nucleotide binding and selectivity. To preserve the overall fold of the rod CNG channel, the equivalent residue of the α subunit of the bovine olfactory channel was substituted into the bovine rod α subunit binding domain in the desired location. In addition to the single substitutions, double and triple mutants were generated and mutant channels were expressed in tsA201 cells. Substitution of F533, K596, and D604 of the bovine rod channel with tyrosine, arginine, and glutamate, respectively, resulted in changes in cGMP and cAMP activation. Analysis of the data using thermodynamic cycles showed that these residues were energetically coupled, suggesting that changes in one residue alter the cGMP contacts with another residue. Competitive coupling between the energetically favorable effects of adding Ni^{2+} to the cytoplasmic face of the channel and replacing F533 with tyrosine suggest that F533 communicates with the C-linker region of the channel, the region previously shown to be required for Ni^{2+} potentiation (*29*). Finally, cAMP-activated currents were enhanced 8−12-fold when K596 was replaced with arginine, suggesting that residue 596 directly influences channel gating.

MATERIALS AND METHODS

Mutagenesis. The bovine retina CNG channel α subunit cDNA was a generous gift from W. Zagotta. The clone was sequenced and modified by deleting the first 175 bp, removing several possible upstream start sites according to the Genbank sequence X51604. The clone was inserted into the vector pAlter-1 by Promega so that single-stranded DNA mutagenesis could be performed according to the protocol of Promega. Mutagenesis was performed to make the singly substituted mutants F533Y, K596R, and D604E. These mutants were restricted and recombined to generate the double and triple mutants. The region from 1440 to 2260 bp involving the mutations was sequenced and then cloned into a large fragment of the original cDNA between the *Nsi*I site at bp 1452 and the *Apa*I site at bp 2244. The mutant cDNA was cloned into the vector pRK-5, a generous gift from K. Dietmar in R. Reed's laboratory, to allow expression in eukaryotic cells.

Expression. The clones were expressed in either tSA-201 cells or COS-1 cells. The transfection was carried out using the LiptofectAMINE method of Gibco/BRL. Briefly, ~2 μg of total cDNA was added to 12 μL of LipofectAMINE Reagent in serum-free DMEM media. The solution was added to 2.5×10^5 cells that were allowed to grow overnight on glass coverslips in six-well plates. After incubation for 5 h, an equivalent amount of 20% serum DMEM media was added. The cells were allowed to incubate in 4.5% CO_2 for 48−72 h before electrophysiological experiments were conducted. The 2 μg of DNA consisted of 1 μg of channel clone; 0.6 μg of green fluorescent protein in the vector pRK-7, a generous gift from S. Lenz; and 0.4 μg of pAdvantage vector form Promega. Inside-out patches were excised from fluorescent cells ~72 h following transfection. The patches were tested for cGMP-activated currents using saturating concentrations of cGMP.

Current Measurements. The bath and electrode solutions used for patching contained 120 mM NaCl, 5 mM Hepes (pH 7.2), 2 mM EDTA, and 2 mM EGTA. Transfected cells, grown on round glass coverslips, were placed in the bottom of a chamber as previously described for photoreceptors (*30*). Corning 0010 glass micropipets with resistances of 10−12 MΩ were used to obtain inside-out patches from fluorescent cells expressing green fluorescent protein. Approximately 10% of the cells were fluorescent, but >90% of the fluorescent cells exhibited cGMP-activated currents following transfection. The patch clamp amplifier output from a Dagan 8900 amplifier was low-pass filtered at 1 kHz (eight-pole Bessel) before being displayed on an oscilloscope and digitization by a personal computer using an Axopatch A/D converter. Voltage pulses lasting 160 ms were applied in 20 mV steps from −80 to 80 mV using an Axopatch Digidata 1200 instrument. Initially, each patch was tested for the presence of CNG channels by measuring the current at saturating cGMP levels. For responsive patches, dose−response data were collected once the maximal response had stabilized, usually within 5 min. Patches usually were stable for 30 min to 1 h.

The currents at each voltage were averaged for at least 100 ms, and the average value was used to construct the current versus voltage (IV) curve. Currents in the absence of nucleotide were subtracted, and the net current was plotted

as a function of nucleotide concentration. All concentration−response data were fitted with a nonlinear algorithm in Tablecurve 4 (Jandel) using the Hill equation, eq 1.

$$I = \frac{I_{max}}{1 + \left(\frac{K_{0.5}}{L}\right)^{N_h}} + A \quad (1)$$

where I is the measured current, I_{max} is the maximal current elicited at saturating concentrations in the patch, L is the concentration of the applied nucleotide, $K_{0.5}$ is the ligand concentration at half-saturation, N_h is the index of cooperativity, and A is the baseline current.

A Student's t test was used for comparing data. In the figures, a confidence of >95% is indicated by a single asterisk (*) and a confidence of >99% is indicated by two asterisks (**).

Molecular Modeling. Molecular modeling was carried out as described previously (*27*, *31*). Briefly, molecular models of the mutant CNG channel binding domains were generated from the bovine retina CNGC model II. Changes in amino acid side chains were followed by minimization of the bond, angle, and geometric terms, and then the total energy (which includes nonbonded terms) was minimized twice using the program AMMP (*32*). The water coordinating the hydrogen bonds between T560 and cGMP was added and restrained for all models, including the anti conformations of the cyclic nucleotides. Manual adjustment of side chains followed the initial energy minimization. Both syn and anti conformations of cGMP and cAMP were tested in all models, and the conformational energy was determined by measuring the interaction energy between ligand and binding domains using AMMP.

The energy minimizations were run on a Silicon Graphics Indigo2 workstation using the program AMMP. The visualization and side chain manipulations were carried out on the Silicon Graphics Indigo2 workstation using InsightII by BioSym.

RESULTS

Mutations in Residues 533, 596, and 604 Affect the $K_{0.5}$ for cGMP. Mutations in the α subunit of the bovine rod CNG channel were introduced at F533, K596, and D604. The corresponding amino acids from the α subunit of the bovine olfactory CNG channel, Y510, R573, and E581, were substituted at each position, respectively. In addition to the single-residue substitutions, mutations with double- and triple-residue substitutions were generated. The single mutation species are F533Y, K596R, and D604E where the first letter denotes the residue in the wild-type rod channel and the last letter denotes the residue from the olfactory channel. The doubly substituted mutants are F533Y/K596R, F533Y/D604E, and K596R/D604E. The triple mutant is denoted F533Y/K596R/D604E.

Mutant and wild-type cDNAs were transfected into tsA201 cells as described in Materials and Methods. Cells expressing green fluorescent protein as a marker were selected for patching and excised, and inside-out patches were tested for cGMP-activated currents. In cells expressing CNG channels, the cGMP-activated currents varied from <50 pA to >1 nA with typical currents of ∼100−300 pA; patches with currents at saturating concentrations of cGMP of <50 pA were not studied. The IV relationships recorded from the wild-type and mutant channels were essentially ohmic as shown in a representative patch from the D604E mutant in Figure 1A. No obvious changes in the IVs were seen with any of the mutants, suggesting that substitution of these residues did not alter the voltage dependence of the channel gating and the mutations did not restore the rodlike outward current rectification.

Our present understanding of the single-channel properties and the kinetics of the CNG channel behavior is too limited to impose many constraints on kinetic models of the channel reaction scheme (*33*, *34*). Recognizing that the dose−response data obtained from macroscopic patch current recordings reflect multiple binding equilibria as well as equilibria for channel gating transitions, we fitted our data with the empirical Hill model. Figure 1B shows representative dose−response curves from single patches of the wild-type channel and the F533Y and D604E mutants illustrating the typical shifts seen in the $K_{0.5}$ values for cGMP. The $K_{0.5}$ value for the F533Y mutant was 38 μM, less than half of the wild-type value which was 86 μM, and the $K_{0.5}$ for D604E was 177 μM. The mean $K_{0.5}$ and N_h values for cGMP for all mutants are presented in Table 1.

The influence of the mutations on the interaction with cGMP can be seen by comparing the mean $K_{0.5}$ values for all the mutants to that of the wild-type channel. Results in Figure 1C show that three mutants, F533Y, K596R, and F533Y/K596R, have $K_{0.5}$ values significantly lower than that of the wild-type channel. The mutants D604E and F533Y/D604E have $K_{0.5}$ values significantly higher than that of the wild-type channel, while mutants K596R/D604E and F533Y/K596R/D604E show no significant change with respect to the wild-type $K_{0.5}$. Generally, replacing D604 with glutamate resulted in an increase in the $K_{0.5}$, while the magnitude of the change was modified by the residues in positions 533 and 596. Replacing F533 with tyrosine or K596 with arginine decreased the $K_{0.5}$ for cGMP, and the doubly substituted mutant F533Y/K596R exhibited the lowest $K_{0.5}$.

On the basis of the $K_{0.5}$ measurements, we can ask several questions about the interaction of cGMP with the rod channel. First, do individual amino acid replacements at positions 533, 596, and 604 affect the interaction of cGMP with the binding domain? Second, do the olfactory residue substitutions result in more favorable or less favorable interactions with cGMP? Third, how are the mutations affected by potentiation with Ni^{2+} and protonation? Finally, is the mutation at one location energetically coupled with a change at another location, or do the residues act independently? To address these questions, we have used a thermodynamic cycle in which the mean $K_{0.5}$ value for each mutant species was converted to an energy of interaction using the relationship $\Delta G = -RT(\ln 1/K_{0.5})$, where R is the ideal gas constant and T is the temperature in kelvin. This approach is similar to previous mutant cycling analyses (*35*−*38*), except that energies derived from the $K_{0.5}$ values reflect multiple equilibria. The term thermodynamic cycle is used to reflect the extension of the previous mutant cycle analysis to include potentiation with Ni^{2+}, protonation, and nucleotide activation.

A mutant thermodynamic cycle for cGMP is shown in Figure 1D, where each corner represents a channel species.

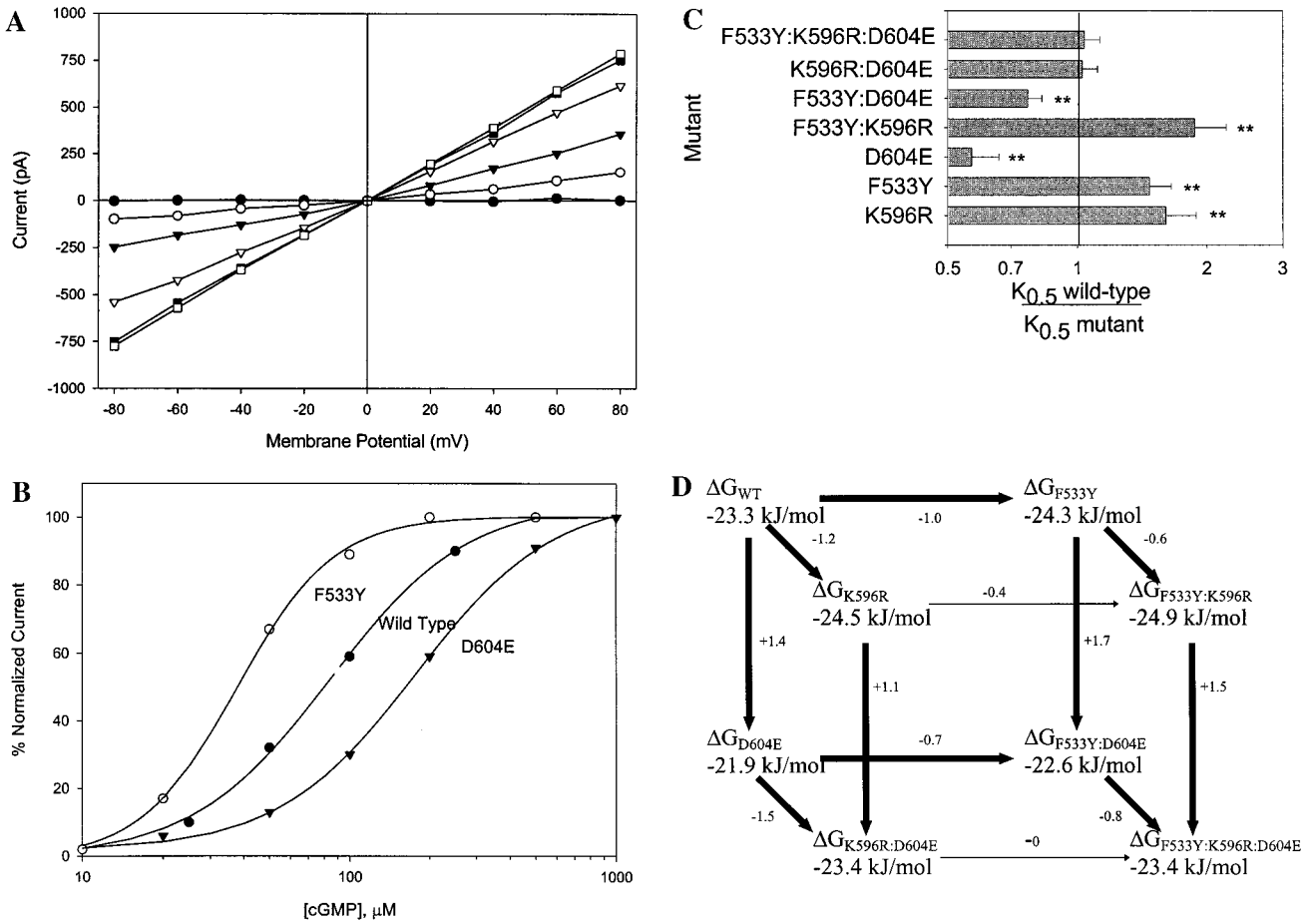

FIGURE 1: Mutations in residues 533, 596, and 604 affect cGMP activation in homomeric α subunit CNG channels. (A) IV relations as a function of cGMP concentration. Currents were recorded under voltage-clamp conditions in an excised inside-out patch from a tsA-201 cell transfected with cDNA for an D604E mutant of the rod CNG channel. The background current recorded in the absence of cGMP was subtracted at each point. The net cGMP-activated currents were activated with 20 (●), 50 (○), 100 (▼), 200 (▽), 500 (■), and 1000 (□) μM cGMP added to the bath. The shape of the IV is nearly linear, and little voltage dependence is seen in the cGMP activation. (B) Mutations at positions 533 and 604 shift the $K_{0.5}$ for cGMP. Currents were measured at 60 mV in the presence of the indicated cGMP concentrations and normalized to the maximal cGMP-activated current in each patch. Data from the wild type (●) and F533Y (○) and D604E (▼) mutants were fitted to the Hill equation, indicated by the solid lines. The single mutant F533Y has a $K_{0.5}$ of 38 μM and an N_h of 2.37; the wild type has a $K_{0.5}$ of 86 μM and an N_h of 1.75, and the D604E mutant has a $K_{0.5}$ of 177 μM and an N_h of 1.62. C. $K_{0.5}$ values for all but two mutants are significantly different from that of the wild-type channel. (C) The $K_{0.5}$ values of the mutants are compared to that of the wild type by taking the ratio of the $K_{0.5}$ values. The standard error of the mean (SEM) is indicated by the error bars. A double asterisk (**) indicates a 99% confidence that the two measurements are significantly different using the Student's t test, and a single asterisk (*) indicates a 95% confidence. (D) Thermodynamic cycle of mutations at positions 533, 596, and 604. Each point of the cube represents a CNG channel species. The energy associated with each species was derived from the $K_{0.5}$ of cGMP using the formula $\Delta G = -RT(\ln 1/K_{0.5})$, with RT being ~2.5 kJ/mol. To determine the effect of a mutation on the interaction with cGMP, the $\Delta\Delta G$ is determined by subtraction. Negative energies reflect an energetically favorable interaction with the ligand, and positive energies reflect an energetically unfavorable interaction. In the cycle, $\Delta\Delta G$ values are given in the direction indicated by the arrow. The thin lines represent changes of 0.4 kJ/mol or less, and the thick lines represent changes of at least 0.5 kJ/mol.

Table 1: Values of the Hill Equation Fit for cGMP[a]

	cGMP			cGMP and Ni^{2+}			cGMP at pH 5.5				
	$K_{0.5}$	N_h	n	$K_{0.5}$	N_h	n	$K_{0.5}$	N_h	n	$\%I_{max}$	n
wild-type	88.2 ± 5.5	2.3 ± 0.12	5	35.4 ± 6.26	1.6 ± 0.06	5	37 ± 9.5	1.34 ± 0.04	2	91 ± 1.5	2
F533Y	60 ± 7.9	2.3 ± 0.4	7	41 ± 6.4	2.45 ± 0.62	3	32 ± 12	1.28 ± 0.31	3	83 ± 11	4
K596R	55 ± 9.0	1.84 ± 0.06	6	13.9 ± 1.84	1.58 ± 0.22	2	21.6 ± 4.8	1.8 ± 0.23	3	87 ± 4.3	3
D604E	155 ± 22	1.58 ± 0.24	3	51 ± 25	1.75 ± 0.15	2	51 ± 1.2	1.71 ± 0.1	2	84 ± 3.5	2
F533Y/K596R	47 ± 18	2.24 ± 0.26	5	27.5 ± 2.6	2.15 ± 0.25	2	40 ± 9.2	1.78 ± 0.23	3	85 ± 3.9	3
F533Y/D604E	115 ± 5.3	2 ± 0.12	8	18.4 ± 4.4	2.57 ± 0.13	2	47 ± 7	1.33 ± 0.29	2	94 ± 3	2
K596R/D604E	86 ± 5	2.15 ± 0.31	4	33 ± 10.4	2.17 ± 0.07	3	42 ± 12	2.17 ± 0.03	2	90 ± 4.9	2
F533Y/K596R/D604E	85 ± 5	2.8 ± 0.23	5	14.9 ± 8.1	0.93 ± 0.28	2	64 ± 7	1.92 ± 0.33	4	81 ± 6.4	7

[a] Dose−response curves were averaged from cGMP activation in normal buffer and with the addition of 5 μM Ni^{2+} or protons. Details are presented in Materials and Methods. $K_{0.5}$ and N_h are the parameters derived from the Hill model, and n is the number of measurements.

The energy changes, $\Delta\Delta G$, are determined by subtracting the values along one edge of the cube. The sign of the energy change indicates whether the changes are energetically favorable (negative values) or unfavorable (positive

values) as determined by the direction of movement at each edge. The singly substituted mutants F533Y and K596R both reflect energetically favorable changes of −1 and −1.2 kJ/mol, respectively, whereas the substitution of glutamate for aspartate in the D604E mutant results in an unfavorable change of 1.4 kJ/mol. These results support the previous predictions that olfactory residues Y510 and R573 interact more favorably with cGMP than the corresponding residues of the rod channel, F533 and K596 (*27*). The energetically unfavorable change with the D604E mutant was not predicted and will be discussed in the molecular modeling section.

Before the effects of multiple mutations in the binding site are examined, it is necessary to establish that a thermodynamic cycle accounts for the major energetic contributions being evaluated. For the cycle to be valid, movement from one species to another must give the same total energy change independent of the path. In the case of a double mutant such as F533Y/K596R, the difference in energy between the wild-type channel, ΔG_{WT}, and the double mutant, $\Delta G_{F533Y/K596R}$, must be independent of the order of the mutations. For example, $\Delta G_{F533Y/K596R} - \Delta G_{WT} = (\Delta G_{F533Y/K596R} - \Delta G_{F533Y}) + (\Delta G_{F533Y} - \Delta G_{WT}) = (\Delta G_{F533Y/K596R} - \Delta G_{K596R}) + (\Delta G_{K596R} - \Delta G_{WT})$. Substituting the energies into this expression gives an energetically favorable interaction of −1.6 kJ/mol for both paths. The analysis can be extended to any two points on the cube in Figure 1D, demonstrating the validity of the thermodynamic cycling analysis for these mutants.

Thermodynamic analysis can now be extended to determine whether the interactions of amino acid residues with cGMP are energetically coupled or independent of each other (*35*). The term coupling encompasses both direct interactions between amino acids and interactions propagated though the protein or the ligand indirectly. A full analysis of this treatment has been presented elsewhere (*37*). To determine whether interactions are coupled, one examines parallel paths in the thermodynamic cycle. If two mutations are independent, the parallel paths are identical and one residue does not influence the other. For example, if the parallel paths of $\Delta G_{WT} - \Delta G_{F533Y}$ and $\Delta G_{K596R} - \Delta G_{F533Y/K596R}$ give the same $\Delta\Delta G$ values, then tyrosine and arginine interactions with cGMP are independent. The cycle in Figure 1D shows, however, the energy differences are not equal; therefore, the interactions of residues 533 and 596 with cGMP are energetically coupled.

The full cycle in Figure 1D shows that substituting one residue affects the interaction with cGMP at the other positions. The cycle also shows that the residues are coupled, and the apparent coupling energy varies between different pairs. This result has several important implications for understanding nucleotide discrimination in CNG channels. First, previous molecular modeling predicted that these three residues interact with the purine, and this prediction is experimentally supported (*26*, *27*). Second, we predicted that the residues at these positions in the rod and olfactory CNG channels differ in the strength of their interactions with cGMP and that these differences are important in ligand discrimination between the channel types. The thermodynamic cycle supports this prediction. Energetic coupling of residues that contact the purine might be expected to affect the conformation of the cyclic nucleotide in the binding site as previously predicted, and this will be discussed in the modeling section of the Results. We next examine the effects of Ni^{2+} potentiation on these mutants in an effort to explore the effects of the mutations on channel gating.

Potentiation of cGMP Activation by Ni^{2+}. The changes in the $K_{0.5}$ values for cGMP induced by the mutations in the rod CNG channel binding domain could be due to changes in cGMP binding, changes in the channel opening, or contributions from both. Although single-channel recordings might reveal the effects of the mutations on the channel opening characteristics, rod channels have small conductance states and rapid open−closed transitions between the states, making these measurements technically challenging (*2*). We have therefore used an indirect approach to determine whether the mutations affect the open probability (P_o) of the channel at saturating concentrations of cGMP. This approach exploits the ability of low concentrations of cytoplasmic Ni^{2+} to increase the P_o at subsaturating cGMP concentrations and defines the maximal P_o of the channels in a given macroscopic patch as shown previously (*29*, *39*).

Currents were recorded in the presence of a saturating level of cGMP and 5 μM Ni^{2+} for all mutants. Without exception, the maximal current in the presence of Ni^{2+} differed by less than 10% from the maximal current measured in the absence of Ni^{2+}, showing that the maximal P_o is achieved at saturating cGMP concentrations. This suggests that channel gating at saturating concentrations of cGMP is not affected by any of the mutations. For comparison, it should be noted that in a previous study (*40*), D604 mutations were generated in which saturating cGMP concentrations did not produce the maximal P_o for the patch.

Representative dose−response curves for cGMP and Ni^{2+} are shown for a single patch of the F533Y/D604E mutant in Figure 2A. In this patch, the $K_{0.5}$ shifted ~6-fold from 122 μM, in the absence of Ni^{2+}, to 23 μM in the presence of Ni^{2+}. Mean $K_{0.5}$ values for cGMP in the presence of Ni^{2+} are given in Table 1 for all mutants. We can now apply the thermodynamic cycle with Ni^{2+} and a single mutation to determine whether the mutation and the allosteric effect of Ni^{2+} are independent or are energetically coupled. Panels B and C of Figure 2 show the thermodynamic cycle for K596R and F533Y, respectively. Figure 2B shows that the parallel sides of the square are not equal but have the same sign; hence, the effects of Ni^{2+} and the substitution of arginine for K596 are energetically coupled. In the previous cycles shown in Figure 1D and Figure 2B, all parallel paths had the same sign, but in Figure 2C, we observe that the signs of two of the parallel sides are opposite. This result shows that the substitution of F533 with tyrosine is energetically favorable in the absence of Ni^{2+}, but in the presence of Ni^{2+}, the substitution is energetically unfavorable. To account for the situation where the signs along parallel paths are opposite, we have used the term competitive coupling. In competitive coupling, the energetically favorable substitution of tyrosine for F533 ($\Delta\Delta G = -1.0$) competes with the energetically unfavorable effect of the mutation in the presence of Ni^{2+} ($\Delta\Delta G = 0.3$). Two possible causes for this competitive effect are (1) the fact that the energetically favorable effect of Ni^{2+} on cGMP interactions with the wild-type channel is partially or fully duplicated by the mutation or (2) the fact that the mutation inhibits the allosteric effects of Ni^{2+}. The implications of this result will be considered

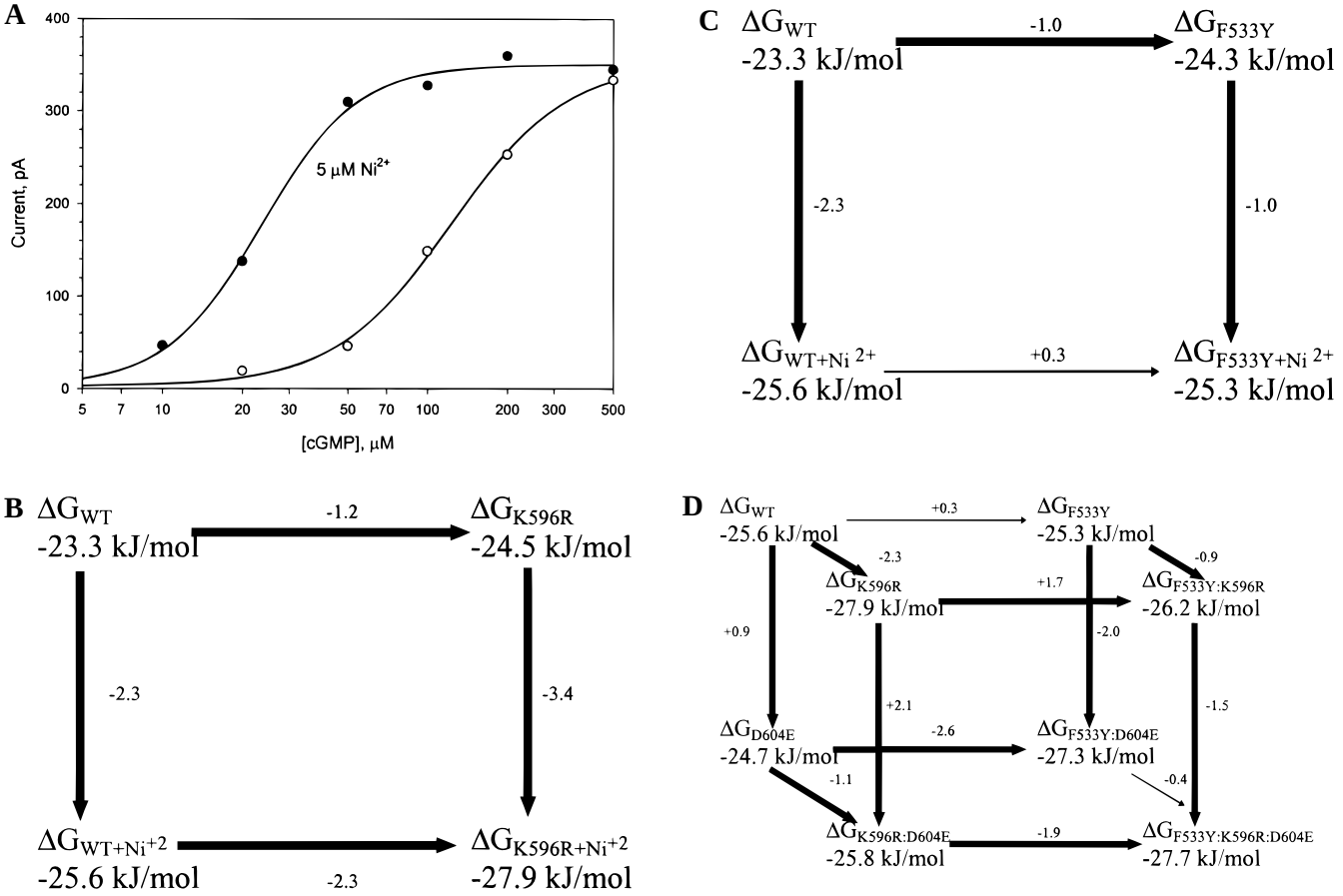

FIGURE 2: Allosteric effects of Ni^{2+} on cGMP activation. (A) Ni^{2+} at 5 μM decreases the $K_{0.5}$ of cGMP in the double mutant F533Y/D604E. Dose−response curves were measured for the F533Y/D604E mutant in a single patch with the normal divalent-free buffer (○) and in buffer containing 5 μM Ni^{2+} (●). The presence of Ni^{2+} shifted the $K_{0.5}$ from 122 μM cGMP with an N_h of 1.97 to 23 μM with an N_h of 2.70. No significant change was seen in the maximal currents produced in the presence of Ni^{2+}. (B) Ni^{2+} and the single mutant K596R show noncompetitive energy coupling using thermodynamic cycling. A thermodynamic cycle comparing the effect of mutating K596 to arginine and the addition of 5 μM Ni^{2+}. The Ni^{2+} and mutation show a noncompetitive energy coupling since all the sign changes in the parallel paths are the same. (C) Ni^{2+} and the single mutant F533Y show competitive energy coupling using thermodynamic cycling. A thermodynamic cycle compares the effect of mutating phenylalanine at position 533 to tyrosine and the addition of 5 μM Ni^{2+}. The Ni^{2+} and mutation show a competitive coupling of energy since the signs of energy change in one of the parallel paths reverse sign. (D) The amino acids at position 533, 596, and 604 are dependently coupled in the presence of 5 μM Ni^{2+} and cGMP. Each point of the cube represents a CNG channel species with the $K_{0.5}$ converted to kilojoules per mole. The numbers on the connecting lines represent the change in energy between the species (moving along the arrows). Amino acid residues at positions 533 and 604 are competitively coupled. The rest of the thermodynamic cycle is noncompetitively coupled.

in the context of previous ligand studies and molecular modeling in a later section.

Extension of the thermodynamic analysis of Ni^{2+} potentiation with single substitutions at each position (data for position 604 not shown) indicates that only the replacement of F533 with tyrosine is competitive with the energetically favorable changes conferred by the addition of Ni^{2+}. A full thermodynamic cycle in the presence of Ni^{2+} is shown in Figure 2D. When this cycle is contrasted with the cycle in Figure 1D in the absence of Ni^{2+}, it can be seen that Ni^{2+} alters the residue coupling. In the absence of Ni^{2+}, residues 533, 596, and 604 are noncompetitively coupled, but in the presence of Ni^{2+}, residues 533 and 604 are competitively coupled.

Effects of Protonation on cGMP-Activated Currents in the Mutant CNG Channels. Protonation has been shown to decrease the $K_{0.5}$ for cGMP and partially block the current at saturating cGMP concentrations (*41*, *42*). Single channel measurements showed that the decrease in nucleotide-activated currents was due to permeation block rather than to a decrease in the P_o (*43*). Additional molecular insights about channel gating and binding have been derived from analysis of cGMP activation in solutions with a reduced pH (*42*−*44*). We therefore examined the effects of protonation on cGMP activation for all mutants to determine the influence of protonation on each residue substitution. Representative data from the K596R mutant (Figure 3A) showed a decrease in the $K_{0.5}$ for cGMP at pH 5.5 from 58 μM at pH 7.2 to 18 μM. The 10−15% decrease in the maximal current at pH 5.5 was seen in all channels and reflects the partial, proton-induced current block. All mutants exhibited a decrease in I_{max} and $K_{0.5}$ at pH 5.5, and the mean values are given in Table 1.

A thermodynamic cycle was used to examine the effects of protonation on the mutants (Figure 3B). By comparing the effects of the single substitutions in the absence (Figure 1D) and presence (Figure 3B) of protonation, we see that the arginine replacement of K596 is energetically unfavorable if tyrosine occupies position 533. This is the only situation where the substitution of arginine results in an energetically

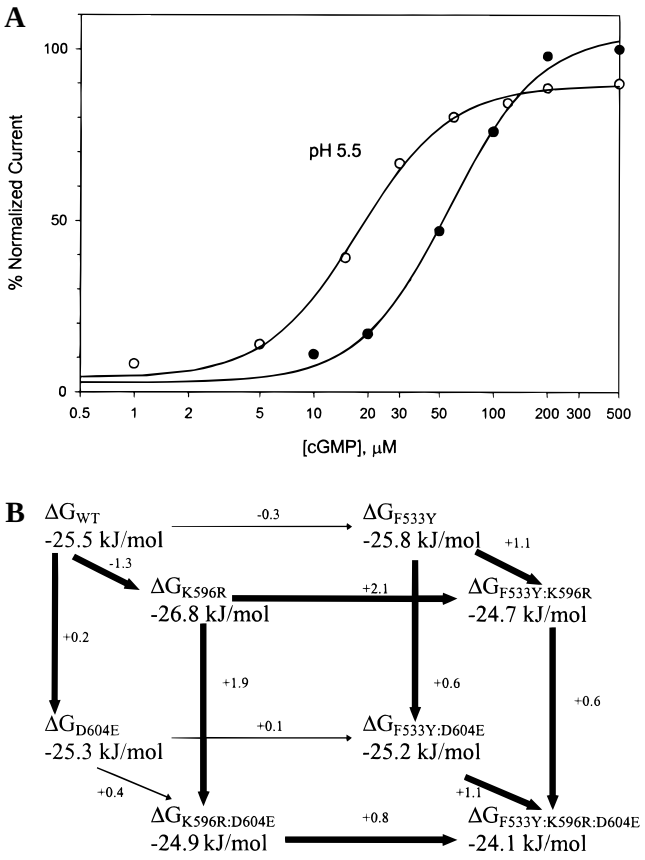

FIGURE 3: Protonation effects of cGMP binding and activation in the bovine rod α subunit mutants. (A) Protonation decreases the $K_{0.5}$ for cGMP and produces a small decrease in the maximal current. cGMP dose−response relations were measured in two different patches in an K596R mutant. At pH 5.5 (○), the $K_{0.5}$ was 18 μM with an N_h of 1.69, and at pH 7.2 (●), the $K_{0.5}$ was 58 μM with an N_h of 1.70. The 10−15% decrease in the normalized current at pH 5.5 compared to that at pH 7.2 was seen in all mutants. (B) The thermodynamic cycle of the residues in positions 533, 596, and 604 is energetically coupled at pH 5.5. In the presence of phenylalanine in position 533, residues 596 and 604 are competitively coupled, as are residues 533 and 596 in the presence of aspartic acid in position 604, and residues 533 and 604 in the presence of lysine in position 596. Residues 596 and 604 are independently coupled in the presence of tyrosine in position 533.

unfavorable interaction with cGMP. Energy-minimized models of the mutant CNG channel binding domains, presented in a later section, suggest an explanation for this finding. Also apparent from the cycle shown in Figure 3B is the effect of substituting glutamate for D604 which is independent of whether arginine or lysine occupies position 596 if tyrosine occupies position 533. This result is noteworthy because positions 596 and 604 are both predicted to lie on the C α helix and might be expected to be coupled. Overall, the mutant channels have provided evidence that residues 533, 596, and 604 are coupled with respect to their interactions with cGMP and these couplings change with the addition of either Ni^{2+} or protonation.

Interactions of the Mutants with cAMP. In many ways, cAMP is a better ligand than cGMP for testing the effects of replacing F533, K596, and D604 in the rod channel with the residues of the olfactory channel because the most striking differences in nucleotide activation properties between these channels are observed in the presence of cAMP. For example, cAMP activated ∼1% of the maximal cGMP-activated current in heterologously expressed rod channels, whereas in the olfactory channels, cAMP activated 100% of the current (*2*). The $K_{0.5}$ values for cAMP vary more widely between the channel types than do those for cGMP, and the lower values for the olfactory channels suggest that cAMP binds more tightly to the olfactory channel than to the rod channel. This proposed tighter binding has been difficult to monitor directly, however, because differences in the N-S2, pore, and C-linker regions of the rod and olfactory channels all contribute directly to the current measurements used to determine the $K_{0.5}$. In this investigation, we retained the complete fold of the rod channel to focus exclusively on these interactions.

We examined the ability of cAMP to activate current in each of the mutant channels. Small currents were seen with all channels as shown in Figure 4A; however, cAMP activated 8−10-fold larger currents in three of the mutants. These mutants all contained arginine in position 596: K596R, F533Y/K596R, and F533Y/K596R/D604E. This increase in current is consistent with our previous prediction that arginine in position 596 forms an interaction with cAMP stronger than the interaction between lysine and cAMP (*27*). A discussion of this result will be extended in the following section of the Results. This increased current with cAMP in the K596R mutant also shows that arginine 596, in addition to residue 604, directly influences cAMP gating.

To examine the cAMP-activated currents, we took advantage of the large potentiation with cytosolic protonation. In addition to the nonspecific effect seen with both cGMP and cAMP, a cAMP-specific potentiation is seen at reduced pH concentrations when residue 604 is an acidic residue (*44*). Large increases in the currents were seen when the pH of the cytoplasmic side was reduced to 5.5, ranging from a high of ∼75% in the wild type and K596R mutant to a low of ∼20% in the K596R/D604E mutant. Table 2 gives the relative cAMP-activated currents at pH 5.5 for all mutants. The reduced current levels at pH 5.5 the with glutamate substitution for D604 suggest that glutamate interferes with cAMP activation of the channel. $K_{0.5}$ values were determined for cAMP activation at pH 5.5. Figure 4B shows dose−response relationships for the F533Y and F533Y/K596R mutants with $K_{0.5}$ values of 1342 and 445 μM, respectively. The wild-type channel had an average $K_{0.5}$ of 801 μM cAMP at pH 5.5; all average $K_{0.5}$ values at pH 5.5 are given in Table 2. The lowest average $K_{0.5}$ of 432 μM was seen in the F533Y/K596R mutant, and the highest value of 1551 μM was seen in the F533Y/D604E mutant. The elevated $K_{0.5}$ values of the D604E mutant support the concept that cAMP is a poor agonist of the rod CNG channel when glutamate occupies position 604.

For those mutants with cAMP-activated current fractions equal to that of the wild-type channel, a thermodynamic cycle was used to analyze the effects of the mutations. This comparison was possible since there was no evidence that the mutation produced a change in the channel gating. This argument does not hold, however, for the glutamate-containing mutants which exhibit reduced cAMP-activated currents with protonation. Figure 4C shows a cycle with the K596 change to arginine and the F533 change to tyrosine and the double mutation. The analysis shows that the effect of replacing F533 with tyrosine depends on the identity of the residue in position 596. The interaction between

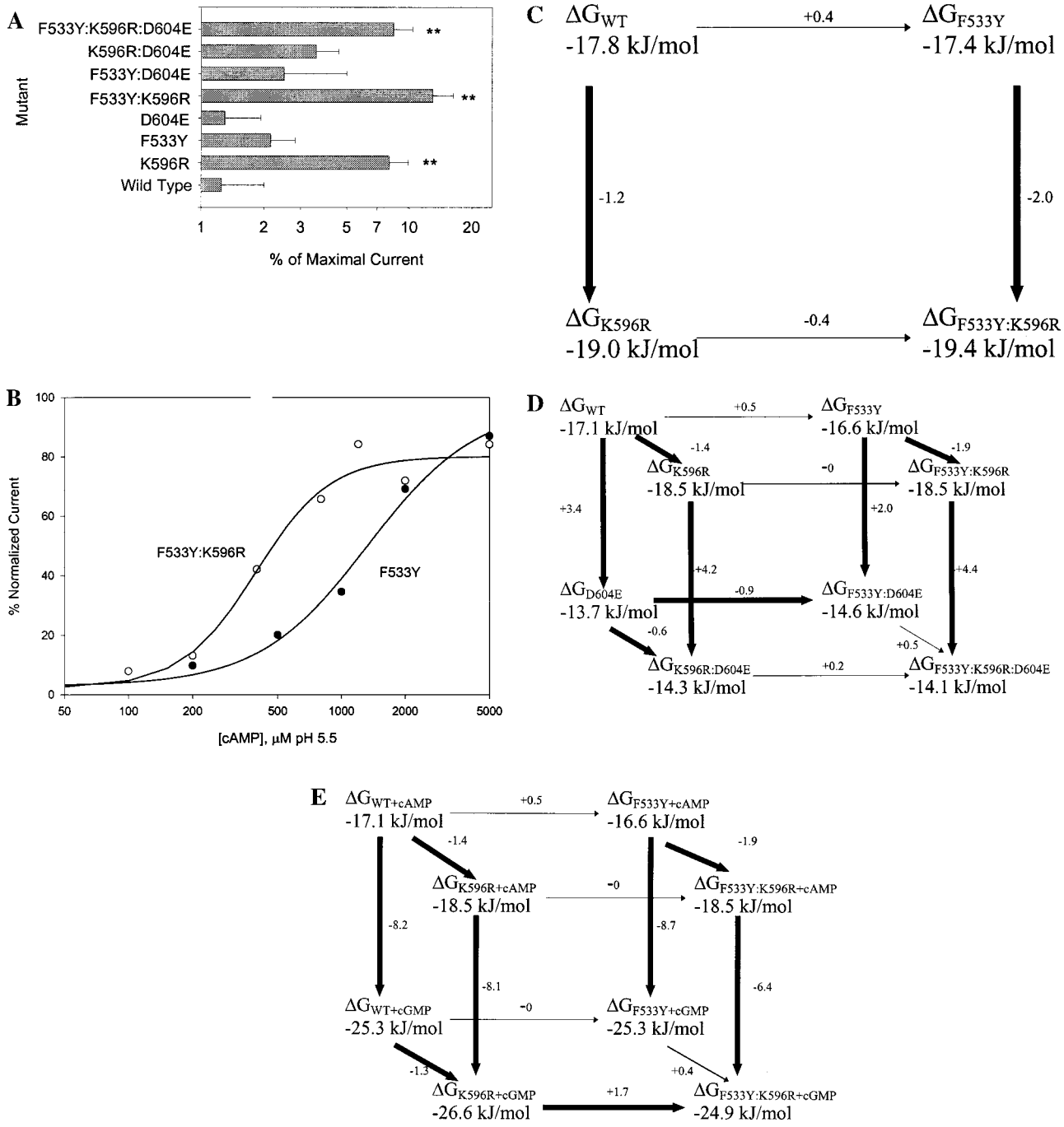

FIGURE 4: Current activation by cAMP in mutant channels. (A) Relative currents produced by cAMP at pH 7.2. The fraction of maximal current produced by 5 mM cAMP was determined by dividing the cAMP-activated current by the maximal cGMP-activated current in each patch. Values for each mutant were averaged and compared to the current produced by the wild-type channels. (B) cAMP dose−response relations for cAMP at pH 5.5 for the F533Y (●) and F533Y/K596R (○) mutant. The $K_{0.5}$ for cAMP at pH 5.5 in the double mutant F533Y/K596R was 445 μM with an N_h of 2.46 and an I_{max} of 78% of saturating cGMP current, and for the mutant F533Y, the $K_{0.5}$ for cAMP at pH 5.5 was 1342 μM with an N_h of 1.66 and an I_{max} of 80%. **(**C) Thermodynamic cycle of residues at position 533 and 596 with cAMP at pH 5.5. Each point of the cube represents a CNG channel species with the $K_{0.5}$ converted to kilojoules per mole. The numbers on the connecting lines represent the change in energy between the species moving along the arrows. The $K_{0.5}$'s adjusted for differences in I_{max} at saturating current levels were not used since the maximal current was nearly the same. Residues at positions 533 and 596 are competitively coupled. (D) Thermodynamic cycle of the residues at positions 533, 596, and 604 in the presence of cAMP at pH 5.5. The $K_{0.5}$'s normalized for differences in I_{max} at saturating current levels were used for this thermodynamic cycle by dividing the $K_{0.5}$ by $\%I_{max}$. The residues at position 533, 596, and 604 are competitively coupled except when phenylalanine is present in position 533, and then residues 596 and 604 are noncompetitively coupled. (E) Thermodynamic cycle of the residues at positions 533 and 596 with cGMP and cAMP. The $K_{0.5}$ values are normalized for differences in I_{max}. This cycle shows that cAMP and cGMP are competitively coupled with residues 533 and 596.

positions 596 and 533 is competitive with cAMP at pH 5.5.

To compare the effects of the mutations on activation by cAMP at pH 5.5, the relative current levels were used to normalize the $K_{0.5}$ values with the expression $K_{0.5}/\%I_{max}$. This normalized parameter, K_{nor}, is analagous to the inverse of k_{cat}/K_M of enzyme kinetics. The thermodynamic cycle was then used to examine the cAMP interactions with the mutants (Figure 4D). The $\Delta\Delta G$ values show that cAMP interactions

Table 2: cAMP Activation of Wild-Type and Mutant CNG Channels[a]

	pH 7.2		pH 5.5				
	$\%I_{max}$	*n*	$\%I_{max}$	*n*	$K_{0.5}$ (μM)	N_h	*n*
wild-type	1.25 ± 0.75	4	75 ± 4	2	801 ± 73	2 ± 0.37	2
F533Y	2.15 ± 0.7	7	69 ± 5.5	4	923 ± 219	1.45 ± 0.13	3
K596R	8.4 ± 2.0	6	77 ± 5.2	4	512 ± 52	1.58 ± 0.39	4
D604E	1.3 ± 0.64	3	24 ± 3.6	3	1042 ± 204	2.39 ± 0.81	2
F533Y/K596R	13 ± 3.3	7	73 ± 8.4	4	432 ± 40	2.34 ± 0.27	3
F533Y/D604E	2.5 ± 2.5	2	57 ± 14.8	5	1551 ± 556	2 ± 0.50	3
K596R/D604E	3.6 ± 1.3	2	21.5 ± 11	4	724	2.26	1
F533Y/K596R/D604E	8.4 ± 2	5	35.4 ± 4.4	5	1291 ± 315	1.92 ± 0.33	2

[a] I_{max} is the relative current elicited by 5 mM cAMP. The maximal current was defined for each patch by saturating concentrations of cGMP at pH 7.2. $K_{0.5}$, I_{max}, and N_h are the parameters derived from the Hill model, and *n* is the number of measurements. Currents were measured at pH 7.2 and 5.5.

are favored with the arginine substitution at position 596 but not the substitution of tyrosine and glutamate at positions 533 and 604, respectively. The cycle also shows that the residues are coupled in their interactions with cAMP; both competitive and noncompetitive changes are seen.

We also asked whether the mutations have similar effects on cGMP and cAMP activation at pH 5.5. The thermodynamic cycle in Figure 4E shows the effects of mutations at positions 533 and 596 at the reduced pH using K_{nor} as described above. The cycle shows that cAMP and cGMP are competitively coupled in their effect at positions 596 and 533. These results are pH-dependent and likely reflect changes in the selection of the ligand conformation at the reduced pH. In the next section, we explore the nature of the contacts predicted between the nucleotide and the binding site for each of the mutant species and predict the dominant conformation of the bound nucleotide on the basis of the predicted interactions with these residues.

Molecular Models of Nucleotide Interactions with the Mutant Channels. The electrophysiological data on the mutant CNG channels support our prediction that residues 533, 596, and 604 interact with bound nucleotides, but the energetically unfavorable interaction of the glutamate substitution at position 604 was not predicted by the earlier modeling of the olfactory binding domain (*27*). To account for packing differences between the rod and olfactory binding domains at locations other than those positions we altered, molecular models were generated for each mutant using AMMP (*32*). The proposed secondary structure of the cGMP binding domain of bovine rod is an eight-stranded β barrel with two C-terminal α helices and an N-terminal α helix (*28*). This motif is illustrated with a model of the F533Y/K596R/D604E mutant binding domain in Figure 5A. In the model, the cyclic nucleotide is surrounded by the binding domain except for the N2 position of cGMP and it is presumed that the nucleotide diffuses to and from the binding site through a pathway between the β5 strand and the C α helix. Several of the predicted contacts between the protein and the nucleotide are shown in detail in panels B and C of Figure 5. The ribofuranose is predicted to make eight contacts with the binding domain as discussed previously (*27*). In addition to these contacts, this region of the binding domain is stabilized by an internal salt bridge between E544 on β6 and K596 on the C α helix. In Table 3, the interactions predicted for each ligand and the range of the interaction are listed.

The conformation of the nucleotide is an important factor in determining the purine interactions with the binding domain since different contacts will be possible depending on whether the nucleotide binds in the syn or anti conformation. Experimentally, the nucleotide conformation can only be determined from a high-resolution structure of the nucleotide bound to the channel; however, molecular modeling is useful because it can lead to testable insights about the conformation-specific contacts between a residue and the purine. Accordingly, we modeled cGMP and cAMP in syn and anti conformations in each of the mutant binding domain models. All models retain the interaction of the N2 group of syn cGMP with T560 via a water molecule. This interaction is a primary determinant for predicting the syn conformation of cGMP and would contribute both enthalpic, via the hydrogen bond formation, and entropic energy because it stabilizes the syn conformation of the bound cGMP. On the β5 strand, F533 is predicted to form a weak interaction with the C6 substituents of both cGMP and cAMP; this interaction is predicted to occur with both syn and anti conformations of the nucleotides. When tyrosine replaces phenylalanine in position 533, the hydroxyl of the side chain is predicted to form a hydrogen bond with either the N1 or N2 position of syn cGMP or the N1 position of syn cAMP. These hydrogen bonds cannot occur with the anti conformation due to the distance between suitable donors and because of packing constraints encountered with V534. This hydrogen bonding interaction would therefore exert a selection for the syn conformation of both cAMP and cGMP. In the K596R mutant, the arginine side chain is predicted to interact with the purine ring and two types of interactions should be possible. A weak, long-range interaction is predicted between the charged arginine and the purine with either ligand in the syn conformation. The decrease in $K_{0.5}$ of cGMP in the K596R mutant compared to that of the wild-type channel is consistent with this prediction. When the ligand is modeled in the anti conformation, a stronger, short-range, interaction is predicted as shown in Figure 5C. With cAMP, this interaction would be expected to minimize the gain of replacing the F533 with tyrosine since the hydroxyl would interact only with the syn conformation of cAMP. In effect, the anti conformation of cAMP is predicted in the arginine-containing mutants when position 533 is phenylalanine. Alternatively, the syn conformation would be preferred when tyrosine replaces the F533 in the presence of arginine 596 since the long-range interaction could occur.

D604 was predicted to interact with cGMP in the syn conformation and cAMP in either the syn or anti conformation. The modeling suggests that the increase in chain length from aspartate to glutamate allows the carboxyl group to

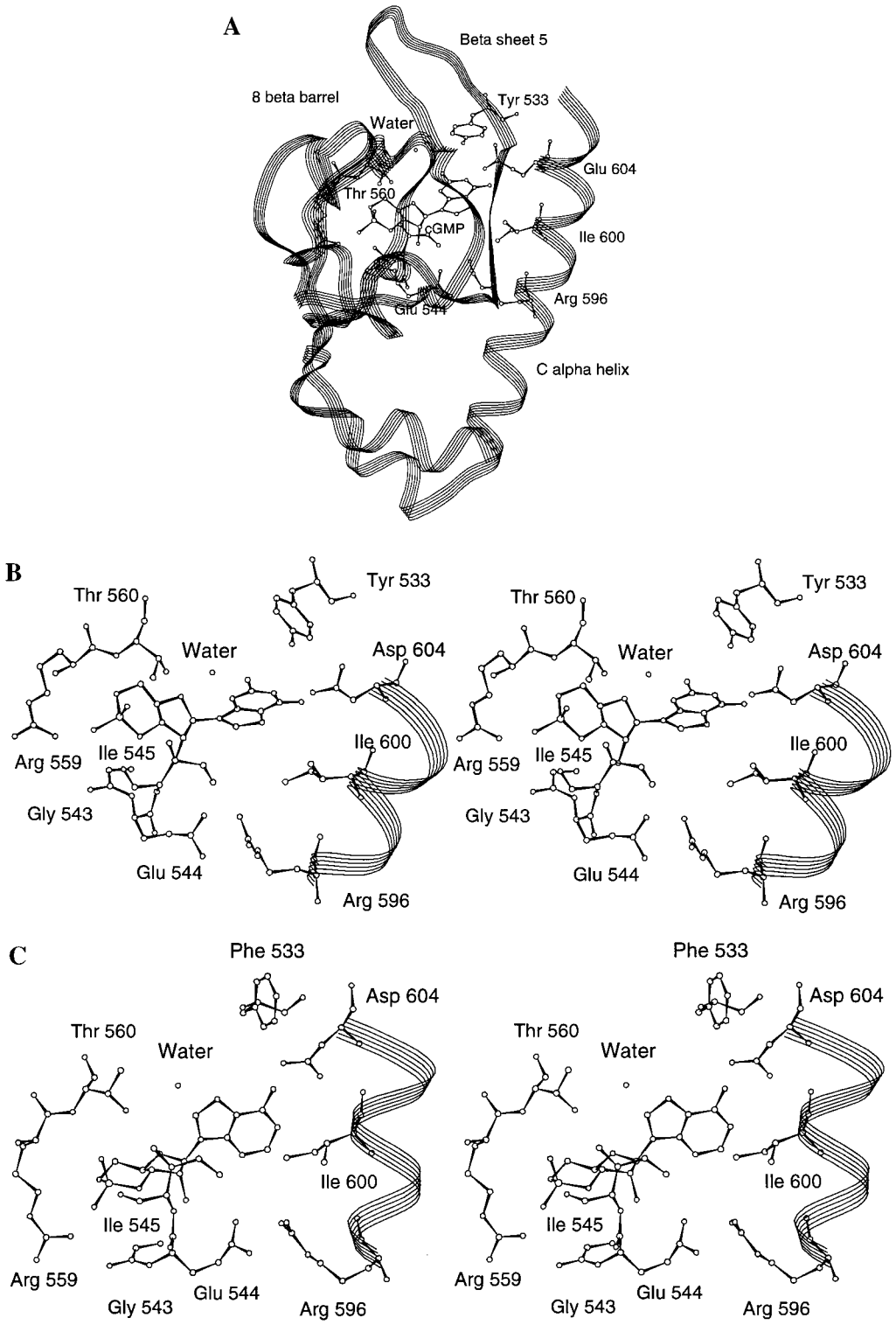

FIGURE 5: Mutant channel molecular models. (A) Ribbon trace of the F533Y/K596R/D604E mutant rod CNG channel binding domain with syn cGMP and selected amino acid residues. The overall structure of the binding domain is an eight-stranded β barrel structure with three α helices. The ribofuranose of cGMP is surrounded by the eight-stranded β barrel. The conformation and binding domain interactions with the ligand are mediated by residues 533 on the β5 strand, 560 on the β7 strand, and residues 596 and 604 on the C α helix. (B) A model of syn cGMP in the binding domain of the mutant F533Y/K596R with selected amino acid residues. The purine ring of cGMP interacts with the four amino acid residues Y533, T560, R596, and D604. Tyr533 OH interacts in hydrogen bonds with the purine rings N1 and N2 located at 3.19 and 3.57 Å, respectively. The Tyr ring is 3.92 Å from O6, and a weak interaction might occur between them. The water mediates an interaction between Thr560 OG1 and cGMP N2. The water molecule is 2.92 and 2.87 Å from each, respectively. The R596 makes a long-range weak interaction with the purine ring, a distance of 5.25 Å, and Asp 604 OD1 and cGMP N1 interact at a distance of 3.24 Å. (C) Anti cAMP in the binding domain of K596R with selected amino acid residues. The purine ring of cAMP interacts with three amino acid residues: F533, R596, and D604. The weak interaction between the ring of F533 and the polar group cAMP N6 occurs at a distance of 3.83 Å. This interaction may be masked somewhat by the charge of D604. R596 interacts with the purine ring of cAMP located 4.65 Å away. The final interaction is a charge bond interaction between Asp 604 OD1 and cAMP N6 which occurs at a distance of 3.02 Å.

Table 3: Predicted Interactions between the Cyclic Nucleotide and the Binding Domain with Distances Given between Two Heavy Atoms

donor	acceptor	distance[g]	type of reaction
61 ring[b]	cGMP 06	3.64−4.29	polar-ring[c]
cAMP N6	61 ring	3.38−3.68	polar-ring
Tyr61 OH	cGMP N1	3.08−3.57	H-bond[e]
Tyr61 OH	cGMP N2	3.10−3.19	H-bond
Tyr61 OH	cAMP N1	2.91−3.52	H-bond
Gly543 N	O2′	2.82−2.91	H-bond
Glu544 N	O2′	2.95−3.05	H-bond
O2′	Glu544 OE1	3.32−3.46	ionic H-bond[d]
Ile545 N	O3′	3.09−3.50	H-bond
Arg559 NH1	O5′	3.41−4.30	ionic H-bond
Arg559 NH1	O7′	3.08−3.21	ionic H-bond
Thr83 N	O6′	3.01−3.33	H-bond
Thr83 OG1	O6′	2.86−3.04	H-bond
water	Thr83 OG1	3.15−3.36	H-bond
cGMP N2	water	2.82−3.00	H-bond
Arg119 NH1	syn purine ring	4.52−5.25	charge-ring[f]
Arg119 NH1	anti purine ring	3.98−4.56	charge-ring
cAMP N1	Glu604 OE1	2.96−3.45	charge density
cAMP N6	Glu604 OE1	2.86−3.33	ionic H-bond
cAMP N6	Asp604 OD1	2.93−3.63	ionic H-bond
cGMP N1	Glu604 OE1	3.17−3.72	ionic H-bond
cGMP N6	Glu604 OE1	3.04−3.47	ionic H-bond
cGMP N1	Asp604 OD1	3.17−3.34	ionic H-bond

[a] Donor is the donor atom in terms of residue type, residue number, and atom type for the noncovalent interaction. Acceptor is the acceptor. Distance is the heavy atom distance. Type is the general type of interaction. [b] The distance between closest atoms where ring systems are involved and not an individual acceptor or donor. [c] A polar-ring interaction is the type between a conjugated ring system and polar atom which is an interaction with approximately half of the energy of hydrogen bonds that can occur at distances of >5 Å (*47*). [d] Ionic H-bond interactions involve a typical hydrogen donor and acceptor and paired with a charged residue, still involves hydrogen, is roughly as strong as a hydrogen bond, and can occur at distances slightly longer than hydrogen bonds. [e] Hydrogen bonds occur at distances of 2−3.5 Å between heavy atoms, have energies of 8−40 kJ/mol, and have a perfect angle of 180° between donor, hydrogen, and acceptor. [f] A charge-ring interaction occurs between a conjugated ring system and a charged residue, can occur at distances of >5 Å, and can have variable energy depending on the angle of interaction and distance (*48*). Charge density is the interaction between electron poor and electron rich areas that does not involve hydrogen, has the same range as a hydrogen bond, and has a variable energy. [g] The distances displayed for the interactions are for all models in which the interaction could occur and are in some cases longer than would normally be considered for that type of interaction. A protein and ligand would maximize these interactions and "draw" the interacting atoms closer together.

extend under the purine ring and interact with N1 and N2 of cGMP and N6 of cAMP in either the syn or anti conformation. In the anti conformation, the longer residue can interact with N1 of cGMP, though this is unlikely to occur because of the preference for the syn conformation. We attribute the increased $K_{0.5}$ values for both cGMP and cAMP in the E604 mutant to packing problems caused by the additional methyl residue of glutamate. Glutamate in the olfactory binding site may pack differently due to the influence of additional residue changes in the local environment that do not interact directly with the ligand.

Models of the double and triple mutants suggest unique interactions not possible in the singly substituted mutants. In the F533Y/D604E mutant, a triad of interactions is predicted between the purine ring in the N1 and C2 positions, the hydroxyl group of tyrosine in position 533, and the carboxyl group of glutamate in position 604. This triad is similar to that predicted for the bovine olfactory binding domain model (*27*). In the bovine rod models, I600 constrains the movement of arginine in position 596, preventing a direct interaction between the arginine and the glutamate in position 604; however, the equivalent $K_{0.5}$ values for the K596R/D604E and F533Y/K596R/D604E mutants suggest a strong combination of interactions not requiring tyrosine.

Interaction energies for both syn and anti conformations of cAMP and cGMP were calculated using AMMP for each mutant, and the results are shown in Table 4. A detailed discussion of these calculations is presented in Scott et al. (*27*). Differences of ≤7 kcal/mol are not considered significant and suggest there is little discrimination among the nucleotide conformations whereas, differences of >7 kcal/mol suggest a conformational preference. As shown in Table 4, the syn conformation of both cGMP and cAMP is predicted when tyrosine is present at residue 533, reflecting the strong interaction between the hydroxyl group and the purine ring. The anti conformation of cAMP is predicted only if arginine replaces K596 and the residue in position 533 is phenylalanine.

DISCUSSION

Mutations of residues 533, 596, and 604 of the bovine rod binding domain of the CNG channel were designed to test the influence of these residues on the interaction with cGMP and cAMP. Each residue was replaced with the corresponding residue from the bovine olfactory CNG channel to determine whether the olfactory residues formed stronger interactions than the corresponding rod residues. The positions were selected on the basis of previous molecular modeling that suggested the residues act together to coordinate the binding of the nucleotide (*26*, *27*). To minimize changes in the overall folds of the protein that might contribute indirectly to nucleotide activation, we altered only these three positions. Our results show that replacing residues 533 and 596 with the corresponding olfactory residue results in an energetically favorable interaction with cGMP; however, replacement of residue 604 with the corresponding olfactory residue is energetically unfavorable. The data also show that the effects of the mutations on cGMP binding are coupled to changes at each of the other positions. D604 was previously shown to influence the nucleotide interaction with the channel (*40*), but this is the first report to show that residues 533 and 596 are important for nucleotide recognition. It is worth noting that these residues would probably not have been selected for site-directed mutagenesis without the molecular models of the rod channel since the modeling predicts contacts with the purine at these positions that are not present in CRP binding to cAMP.

The small $\Delta\Delta G$ changes, ranging from 1 to 4 kJ/mol, observed with the conservative substitutions in the CNG channel binding domain are consistent with these residues playing a role in nucleotide discrimination but making only a small contribution to the total ligand binding energy. In contrast, these values can be compared with the $\Delta\Delta G$ values for mutations of residues predicted to be required for nucleotide binding such as those ribofuranose contacts conserved among all members of the cyclic nucleotide binding domain family. Nonconservative mutations at T560 (*9*) and R559 (*45*) of the rod channel resulted in ∼30- and

Table 4: AMMP Calculated Binding Energies[a]

	cGMP				cAMP			
	syn	anti	$\|\Delta E\|$	prediction	syn	anti	$\|\Delta E\|$	prediction
wild-type	−69.36	−55.86	13.50	syn	−71.59	−69.00	2.59	syn/anti
F533Y	−73.70	−59.20	14.50	syn	−78.20	−70.20	8.00	syn
K596R	−72.00	−47.70	24.30	syn	−73.70	−70.40	3.30	anti*
D604E	−75.50	−47.70	27.80	syn	−74.60	−65.00	9.60	syn
F533Y/K596R	−74.90	−42.20	32.70	syn	−77.70	−71.30	6.40	syn*
F533Y/D604E	−73.70	−57.20	16.50	syn	−77.20	−69.00	8.20	syn
K596R/D604E	−75.20	−53.90	21.30	syn	−72.50	−67.60	4.90	anti*
F533Y/K596R/D604E	−73.70	−57.20	16. 50	syn	−80.60	−70.20	10.40	syn

[a] Syn and anti columns show the calculated energies of interaction for the ligand in each conformation in the binding domain. ΔE is the difference between the calculated syn and anti conformational energy. Absolute energies of >7 kcal/mol (an empirical choice) are considered significant in choosing the ligand conformation. The predicted ligand conformation refers to the most probable ligand conformation according to the calculation except where indicated with an asterisk (*), which indicates that the conformation selection was based on the proposed ligand interactions in the binding domain and not on the calculated ΔE.

~1600-fold decreases in the $K_{0.5}$ values for cGMP, respectively. The $\Delta\Delta G$ value for the R559E substitution is 18.7 kJ/mol, calculated from a wild-type $K_{0.5}$ of 1.8 μM and a mutant value of 3379 μM (*45*), and the $\Delta\Delta G$ change for the T560A mutation is 8.3 kJ/mol, calculated from a wild-type value of 33 μM and a mutant value of 940 μM (*9*). These large changes are consistent with the loss of required hydrogen bonds or salt bridges between the residue and the ribofuranose (*28*). Typical values for a hydrogen bond range from 8 to 40 kJ/mol. T560, in addition to forming a hydrogen bond with the ribofuranose, is predicted to form a hydrogen bond with the purine through a water molecule (*27*). In the case of the mutations at positions 533, 596, and 604, the relatively weak contacts with the purine are predicted to be modified, not lost, after the olfactory substitutions.

Changes in Channel Function Due to Replacement of F533 with Tyrosine. Insights about the role of each residue in channel activation emerge from examining the mutant data. First, we consider the effects of substituting F533 with tyrosine. This aromatic residue is predicted to form a polar-ring bond with the purine. The addition of the hydroxyl in tyrosine increases the strength of this interaction in the models. The energetically favorable change in the interaction with cGMP in the F533Y mutant is consistent with the prediction that tyrosine interacts more strongly than phenylalanine. The most interesting result with the position 533 mutants is that the potentiating effect of Ni^{2+} is greatly reduced when tyrosine replaces phenylalanine. This competitive interaction shows that the presence of tyrosine influences channel activation in a way that may be similar to the Ni^{2+} potentiation. In previous experiments, Ni^{2+} potentiation has been shown to require H420 in the C-linker region of the channel which is located between the final transmembrane segment and the cyclic nucleotide binding domain (*46*). This suggests that the energetically favorable effect of replacing F533 with tyrosine also involves a communication with the C-linker region of the channel. Such a communication could be mediated directly or indirectly, but unlike the effects of Ni^{2+}, this interdomain communication could be physiologically relevant in olfactory channels.

The role of the C-linker region in bovine cone and rabbit olfactory CNG channels was recently explored using a series of chimeras (*8*). The study showed that three residues in the C-linker region contribute directly to the determination of the cAMP efficacy of the cone channel. When the cone channel residues were replaced with the corresponding residues from the olfactory channel, the efficacy of cAMP increased to resemble that of the wild-type olfactory channel and the single channel properties were dramatically altered. Although it is not known how information about the identity of the nucleotide species is conveyed from the binding site to the C-linker region of the channel, our results raise the possibility that the aromatic residue on the β5 strand plays a role in this communication.

It is also instructive to recall that chimera CNG channels formed from bovine rod and catfish olfactory channels showed that the N-S2 domain of the olfactory channel plays a central role in determining the P_o of the rod and olfactory channels and is a major determinant of cAMP efficacy (*19*). As suggested by Zong et al. (*8*), differences in the primary sequences of various family members at multiple locations may be important in determining the relative contribution of different regions of the channel to the gating. Clearly, much remains to be revealed about the interdomain and intersubunit communication in the CNG channel and how the communication affects channel gating.

Changes in Channel Function Due to Replacement of K596 with Arginine. K596 is predicted to lie two turns below D604 on the terminal C α helix of the binding domain. Energy-minimized molecular models of the olfactory binding domain first suggested that this residue might interact with the bound purine (*27*) since similar interactions are not present in either CRP or PKA (*23*, *25*). The energetically favorable change resulting from the replacement of K596 with arginine shows that the olfactory residue interacts with the purine and that the interaction with arginine is stronger than that of K596. The most surprising result with the K596R mutant was the 10-fold increase in cAMP-activated current which was not seen with the other singly substituted mutants. This result shows that residue 596 has a direct influence on channel gating. Further support for the role of arginine in channel gating is shown by the bovine cone CNG channel which has arginine in the position corresponding to 596 (*8*). In heterologous expression, the normalized current activated by saturating concentrations of cAMP in the cone channel is ~20% compared to the ~1% with the bovine rod α subunit homomeric channels.

Since our molecular modeling is restricted to the binding domain and since the role of this residue has not been previously explored, we cannot predict what interactions position 596 might have with other domains of the channel.

Recent evidence that the CNG channel functions as two dimers (*34*) raises the possibility that the C α helices of two subunits communicate directly to form a functional unit. Mutations at the opposite face of the C α helix might reveal more about the cross-talk of this region of the channel.

Changes in Channel Function Due to Replacement of D604 with Glutamate. The major contribution of this study with respect to the role of residue D604 is to show that the interactions between D604 and the bound nucleotide are coupled to the residues in positions 533 and 596. This result provides strong support for our previous molecular modeling predicting that these three residues interact through a number of bonds to stabilize the conformation and position of the nucleotide in the binding site. This coordinated stabilization is consistent with the relatively small $\Delta\Delta G$ values seen with each of the mutations and most likely accounts for the relative nucleotide selectivity between the rod and olfactory channels. The relative current levels, on the other hand, are clearly influenced by other regions of the channel as discussed above.

Mutations in D604 have been examined in a number of previous studies. This residue was an obvious candidate for mutagenesis since the corresponding residue in CRP makes critical contacts with cAMP that enable activation of the DNA binding domain (*25*). Previously, D604 was substituted with an acidic glutamate, a polar glutamine or asparagine, or an uncharged methonine (*40*, *44*). In all cases, replacing the aspartate led to in an increase in the $K_{0.5}$ for cGMP, compared to that of the wild-type channel. Replacing D604 with nonacidic residues resulted in changes in cAMP activation. In the D604Q mutant, saturating levels of cAMP activated nearly as much current as cGMP, and in the D604M mutant, cAMP was a more effective agonist than cGMP. The $K_{0.5}$ values reported for the D604M mutants were in the range of 200−400 μM for both nucleotides, suggesting that cAMP binds as tightly as cGMP and the D604N mutant showed increased $K_{0.5}$ values for both cGMP and cAMP compared to that of the wild-type channel. The D604 mutants demonstrate that the size and chemical nature of the side chain of this residue affect both the binding and gating of the channel. The mutagenesis data with the D604E mutant suggest that in the rod channel, the substitution of glutamate results in unfavorable packing due to the additional methyl substituent. While our data with the D604E mutant are consistent with previous results on D604, our analysis with the other mutants differs from previous interpretations that D604 is the primary determinant of nucleotide selectivity in the rod CNG channel (*40*). Our results provide clear evidence that the contacts with cGMP made by residues 533, 596, and 604 are energetically coupled and no single residue dominates the ligand interaction with the binding domain.

The effects of protonation on the D604 mutants can also be examined in the context of previous experiments. Previously, it was shown that the current increases at subsaturating concentrations of cGMP and cAMP at pH 5.0 required the expression of H468 located in the C-linker region of the channel (*44*). In addition to the relatively small potentiation mediated by H468, protonation produced a cAMP specific effect (*40*, *44*). This potentiation required an acidic residue at position 604 and was absent in the D604 mutants substituted with uncharged polar or nonpolar residues. It was proposed that the negative charge of D604 created an unfavorable electrostatic interaction with the unshared pair of electrons at N1 of cAMP, and this repulsion was relieved by protonation of the acidic side chain (*44*). While this is possible, we suggest an alternative explanation, namely, that protonation of cAMP at the reduced pH alters the charge distribution of the six-membered adenine ring at the N1 position. Depending on the local protein environment, the carboxylic acid side chain of D604 could be protonated at pH 5.5, the pH used in our experiments, but acid titration of cAMP at pH values in the range of 6.0 (unpublished results) shows that protonation of the adenine will occur at this pH. In other words, we propose that the change in the electronic charge distribution of the adenine six-membered ring increases the strength of the interaction between the carboxyl group of D604 and the adenine ring, resulting in changes in cAMP activation. Since the N1 position of cGMP is protonated most of the time due to the electron withdrawal of the C6 keto substituent, the effects of protonation would be more apparent with adenine.

A Dynamic Model of the CNG Channel Binding Domain. The combined data from ligands and channel mutants and the molecular models suggest that two regions of the binding domain are involved in interdomain communications. The first region is the β5 strand containing residue 533, and the second is the C α helix containing both residues 604 and 596. On the basis of the reduction in the cGMP $K_{0.5}$ and the reduced Ni^{2+} allostery seen with the F533Y mutant, we suggest that the β5 strand facilitates channel opening by communicating with regions of the channel involved in gating, including the C-linker region. We therefore propose that the binding site initially "opens" to permit diffusion of the ligand from the cytosol. Support for this concept is taken directly from the co-crystallized cAMP−CRP structure which shows the nucleotide buried within the binding domain (*25*). As the ligand diffuses into the pocket, the contacts with the ribofuranose seat the ligand. These contacts are energetically important as demonstrated by recent experiments showing a 3000-fold increase in the $K_{0.5}$ for cGMP with mutation of an arginine residue (R559 in the bovine rod channel) which is conserved in all cyclic nucleotide binding domain members (*45*) and the large decreases in $K_{0.5}$ for cGMP when T560 was replaced with alanine since T560 is predicted to contact both the guanine and the ribofuranose (*9*). These highly conserved contacts with the ribofuranose are probably not involved in the nucleotide discrimination, and they should not differ between cGMP and cAMP or vary with the conformation of the nucleotide.

Once the ribofuranose is seated, contacts can be established between the purine and residues 533, 560, 596, and 604 and possibly others not yet identified. These contacts most likely stabilize the ligand conformation, depending on the exact nature of the contacts and the ligand involved. Finally and necessarily, the β5 strand and the C α helix come together drawn by the purine contacts with residues 533 and 604. Whatever the nature of the interaction between the C6 substituent of the purine and the binding domain, the inactive 2-amino cPMP shows that some obligatory interaction is mediated by this substituent (*6*). The C α helix may pivot away from the rest of the binding domain in the absence of a ligand, but once the ligand occupies the binding site, the helix communicates with the β5 strand in order for the channel open probability to increase. The molecular model-

ing suggests that the phenyl ring on F533 on the β5 strand is drawn toward the C6−N1 region of the ligand which is interacting with the C α helix through residue 604.

While the details of this model may not be correct, the model provides a framework for future investigations that will ultimately lead to a better understanding of how CNG channels function. In turn, future experiments will provide additional constraints for the molcular modeling leading to more accurate insights into the structure of the cyclic nucleotide binding domain.

ACKNOWLEDGMENT

We thank Dr. Rob Harrison for help with the modeling and Dr. Jim Lear for helpful discussions about the work involving the cAMP protonation. We also thank Drs. Gregg Wells and Irene Weber for their careful reading of the manuscript. Additional information about the molecular modeling can be found at http://athens.dental.upenn.edu/tanaka/index.html. AMMP can be obtained from Dr. Harrison at http://asterix.jci.tju.edu/progs.html.

REFERENCES

1. Fesenko, E. E., Kolesnikov, S. S., and Lyubarsky, A. L. (1985) *Nature 313*, 310−313.
2. Zagotta, W. N., and Siegelbaum, S. A. (1996) *Annu. Rev. Neurosci. 19*, 235−263.
3. Finn, J. T., Grunwald, M. E., and Yau, K. (1996) *Annu. Rev. Physiol. 58*, 395−426.
4. Nakamura, T., and Gold, G. H. (1987) *Nature 325*, 442−444.
5. Zufall, F., Firestein, S., and Shepherd, G. M. (1994) *Annu. Rev. Biophys. Biomol. Struct. 23*, 577−607.
6. Tanaka, J. C., Eccleston, J. F., and Furman, R. E. (1989) *Biochemistry 28*, 2776−2784.
7. Goulding, E. H., Ngai, J., Kramer, R. H., Colicos, S., Axel, R., Siegelbaum, S. A., and Chess, A. (1992) *Neuron 8*, 45−58.
8. Zong, X., Zucker, H., Hofmann, F., and Biel, M. (1998) *EMBO J. 17*, 353−362.
9. Altenhofen, W., Ludwig, J., Eismann, E. W., Bonigk, W., and Kaupp, U. B. (1991) *Proc. Natl. Acad. Sci. U.S.A. 88*, 9868−9872.
10. Dhallan, R. S., Yau, K., Schrader, K. A., and Reed, R. R. (1990) *Nature 347*, 184−187.
11. Nawy, X., and Jahr, C. E. (1991) *Neuron 7*, 677−683.
12. Ahmad, I., Leinders-Zufall, T., Docsis, J. D., Shepherd, G. M., Zufall, F., and Barnstable, C. J. (1994) *Neuron 12*, 155−165.
13. Biel, M., Zong, X., Distler, M., Bosse, E., Klugbauer, N., Murakami, M., Flockerzi, V., and Hofmann, F. (1994) *Proc. Natl. Acad. Sci. U.S.A. 91*, 3505−3509.
14. Weyand, I., Godde, M., Frings, S., Weiner, J., Muller, F., Altenhofen, W., Hatt, H., and Kaupp, U. B. (1994) *Nature 368*, 859−863.
15. Kingston, P. A., Zufall, F., and Barnstable, C. J. (1996) *Proc. Natl. Acad. Sci. U.S.A. 93*, 10440−10445.
16. Dryer, S. E., and Henderson, D. (1991) *Nature 353*, 756−758.
17. Zufall, F., Shepherd, G. M., and Barnstable, C. J. (1997) *Curr. Opin. Neurobiol. 7*, 404−412.
18. Jan, L. Y., and Jan, Y. N. (1990) *Nature 345*, 672.
19. Goulding, E. H., Tibbs, G. R., and Siegelbaum, S. A. (1994) *Nature 372*, 369−374.
20. Gordon, S. E., and Zagotta, W. N. (1995) *Neuron 14*, 857−864.
21. Kaupp, U. B., Niidome, T., Tanabe, T., Terada, S., Bonigk, W., Stuhmer, W., Cook, N. J., Kangawa, K., Matsuo, H., Hirose, T., Miyata, T., and Numa, S. (1989) *Nature 342*, 762−766.
22. Taylor, S. S., Buechler, J. A., and Yonemoto, W. (1990) *Annu. Rev. Biochem. 59*, 971−1005.
23. Su, Y. I., Dostmann, W. R. G., Herberg, F. W., Durick, K., Xuong, N., Ten Eyck, L., Taylor, S. S., and Varughese, K. I. (1995) *Science 269*, 807−813.
24. McKay, D. B., Weber, I. T., and Steitz, T. A. (1982) *J. Biol. Chem. 257*, 9518.
25. Weber, I. T., and Steitz, T. A. (1987) *J. Mol. Biol. 198*, 311−326.
26. Scott, S.-P., and Tanaka, J. C. (1995) *Biochemistry 34*, 2338−2347.
27. Scott, S.-P., Harrison, R. W., Weber, I. T., and Tanaka, J. C. (1996) *Protein Eng. 9*, 333−344.
28. Kumar, V. D., and Weber, I. T. (1992) *Biochemistry 31*, 4643−4649.
29. Gordon, S. E., and Zagotta, W. N. (1995) *Neuron 14*, 177−183.
30. Furman, R. E., and Tanaka, J. C. (1990) *J. Gen. Physiol. 96*, 57−82.
31. Scott, S.-P., and Tanaka, J. C. (1998) *Methods Enzymol. 293*, 620−647.
32. Harrison, R. W. (1993) *J. Comput. Chem. 14*, 1112−1122.
33. Ruiz, M., and Karpen, J. W. (1997) *Nature 389*, 389−392.
34. Liu, D. T., Tibbs, G. R., Paoletti, P., and Siegelbaum, S. A. (1998) *Neuron 21*, 235−248.
35. Horovitz, A., and Fersht, A. R. (1990) *J. Mol. Biol. 214*, 613−617.
36. Carter, P. J., Winter, G., Wilkinson, A. J., and Fersht, A. R. (1984) *Cell 38*, 835−840.
37. Serrano, L., Horovitz, A., Avron, B., Bycroft, M., and Fersht, A. R. (1990) *Biochemistry 29*, 9343−9352.
38. Hidalgo, P., and MacKinnon, R. (1995) *Science 268*, 307−310.
39. Ildefonse, M., Crouzy, S., and Bennett, N. (1992) *J. Membr. Biol. 130*, 91−104.
40. Varnum, M. D., Black, K. D., and Zagotta, W. N. (1995) *Neuron 15*, 619−625.
41. Tanaka, J. C. (1993) *Biophys. J. 65*, 2517−2523.
42. Picco, C., Sanfilippo, C., Gavazzo, P., and Menini, A. (1996) *J. Gen. Physiol. 108*, 265−276.
43. Gavazzo, P., Picco, C., and Menini, A. (1997) *Proc. R. Soc. London 264*, 1157−1165.
44. Gordon, S. E., Oakley, J. C., Varnum, M. D., and Zagotta, W. N. (1996) *Biochemistry 35*, 3994−4001.
45. Tibbs, G. R., Liu, D. T., Leypold, B. G., and Siegelbaum, S. A. (1998) *J. Biol. Chem. 273*, 4497−4505.
46. Gordon, S. E., and Zagotta, W. N. (1995) *Proc. Natl. Acad. Sci. U.S.A. 92*, 10222−10226.
47. Levitt, M., and Perutz, M. (1988) *J. Mol. Biol. 201*, 751−754.
48. Reid, K. S. C., Lindley, P. F., and Thornton, J. M. (1985) *FEBS Lett. 190*, 209−213.

BI981185D